

## Chapter 2

# The Air–Sea Boundary Interaction Zone

The research problem addressed by ambient noise investigators since the 1950s is the quantitative determination of the sources of sound in the sea. Investigators quickly realized the importance of intermittent sources of sound, compared with the persistent ambient background. Biological noises and nonbiological (including man-made sounds) sources were considered intermittent and predicated on the areas of operation of naval sonar systems. Certainly one would observe a cacophony of noises, grunts, moans, chirps, etc. in shallow water and arctic areas. The crustaceans (shellfish, shrimp), marine mammals (whales, killer whales, and dolphins) and many fish (croakers) produce loud sounds and these can often dominate the ambient noise background (see the suggested bioacoustic references in Chapter 1). Nonbiological sources such as atmospheric storms, seismic disturbances, and the activities of man such as fishing, offshore oilrigs, and airgun surveys have been studied and are also important contributors to the noise field. However, this monograph focuses on the *natural physical mechanisms* of ambient noise that determine the persistent ambient noise background and the properties of the air–sea interaction zone that determine the characteristics of this sound.

The sea–surface interaction zone (Fig. 2.1) is characterized by the wave spectrum, an atmospheric boundary layer, and a subsurface boundary layer. The atmospheric boundary layer, the marine layer, depends on the roughness of the surface determined by the sea state spectrum, thermal stability, humidity flux, and wind speed. The subsurface layer depends on the thermal stability, suborbital wave motions, and turbulence below the sea surface but also on the presence of microbubble layers and clouds. Indeed, this complex situation is difficult to characterize experimentally because of lack of knowledge of the boundary layer characteristics, which are difficult to characterize theoretically. Nevertheless, a qualitative description of this interaction zone is possible.

As shown in Fig. 2.1, the interaction zone basically is composed of two-phase turbulent layers: spray splash and air above, with bubble clouds, critters, and water below. The general problem for the air–sea layer is the characterization of the state of the sea and the velocity profile above the rough moving sea surface. The problem in the subsurface layer is the characterization of the convection and the presence of microbubbles as a function of sea state and water column stability.

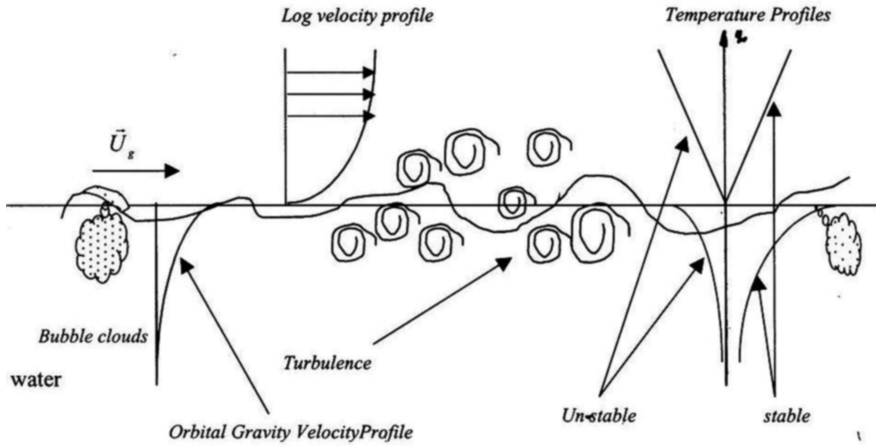


Fig. 2.1 The air–sea interaction zone

## The Marine Boundary Layer

The state of the sea has long been a subject of interest for the mariner. Table 2.1 shows the Beaufort scale along with the Hydrographic Office and international scales. Bowditch's *The American Practical Navigator* (Bowditch (1966)) has been widely used in this regard. A key feature of the Beaufort scale is the combination of the visual appearance of the sea surface as well as the wind speed. The visual observations reflect the understanding that the sea state spectrum, fetch, and various near-surface conditions can have a drastic effect on the real state of the sea. Needless to say, the judgment as to the state of the sea can vary from one observer to the next and consequently one would prefer a standard measurement such as wind speed, water temperature, air temperature, or humidity.

As stated previously, the air–sea interaction zone is composed of two turbulent layers, each layer containing multiple unique features. The basic question is what simplification can be made to characterize the complex zone to adequately parameterize the production of sound; can an analytical model with measured parameters describe the state of this zone and parameterize the production of sound? Wenz in his classic paper wisely chose the Beaufort scale (Table 2.1) with its reliance on wind speed, wave height, and appearance of the sea surface, as the parameterization. This choice incorporates the combined effects of mass, momentum, and heat transfer.

One choice is the selection based on empirical evidence of the logarithmic velocity profile of the marine surface layer. Would a measurement of the wind speed at a reference height, 10 m, and a logarithmic velocity profile be an adequate parameterization of this complicated interaction zone? Experience shows to first order that wind speed is a good descriptor and is widely used; but could the exclusive use of the wind speed descriptor also account for much of the noise variability observed?

Table 2.1 The Beaufort scale

Beaufort number	Wind speed				Seaman's term	World Meteorological Organization (1964)	Estimating wind speed	
	knots	mph	meters per second	km per hour			Effects observed at sea	Effects observed on land
0	under 1	under 1	0.0-0.2	under 1	Calm	Calm	Sea like mirror.	Calm; smoke rises vertically.
1	1-3	1-3	0.3-1.5	1-5	Light air	Light air	Ripples with appearance of scales; no foam crests.	Smoke drift indicates wind direction; vanes do not move.
2	4-6	4-7	1.6-3.3	6-11	Light breeze	Light breeze	Small wavelets; crests of glassy appearance, not breaking.	Wind felt on face; leaves rustle; vanes begin to move.
3	7-10	8-12	3.4-5.4	12-19	Gentle breeze	Gentle breeze	Large wavelets; crests begin to break; scattered whitecaps.	Leaves, small twigs in constant motion; light flags extended.
4	11-16	13-18	5.5-7.9	20-28	Moderate breeze	Moderate breeze	Small waves, becoming longer; numerous whitecaps.	Dust, leaves, and loose paper raised up; small branches move.
5	17-21	19-24	8.0-10.7	29-38	Fresh breeze	Fresh breeze	Moderate waves, taking longer form; many whitecaps; some spray.	Small trees in leaf begin to sway.
6	22-27	25-31	10.8-13.8	39-49	Strong breeze	Strong breeze	Larger waves forming; whitecaps everywhere; more spray.	Larger branches of trees in motion; whistling heard in wires.
7	28-33	32-38	13.9-17.1	50-61	Moderate gale	Near gale	Sea heaps up; white foam from breaking waves begins to be blown in streaks.	Whole trees in motion; resistance felt in walking against wind.
8	34-40	39-46	17.2-20.7	62-74	Fresh gale	Gale	Moderately high waves of greater length; edges of crests begin to break into spindrift; foam is blown in well-marked streaks.	Twigs and small branches broken off trees; progress generally impeded.
9	41-47	47-54	20.8-24.4	75-88	Strong gale	Strong gale	High waves; sea begins to roll; dense streaks of foam; spray may reduce visibility.	Slight structural damage occurs; slate blown from roofs.
10	48-55	55-63	24.5-28.4	89-102	Whole gale	Storm	Very high waves with overhanging crests; sea takes white appearance as foam is blown in very dense streaks; rolling is heavy and visibility reduced.	Seldom experienced on land; trees broken or uprooted; considerable structural damage occurs.
11	56-63	64-72	28.5-32.6	103-117	Storm	Violent storm	Exceptionally high waves; sea covered with white foam patches; visibility still more reduced.	
12	64-71	73-82	32.7-36.9	118-133				
13	72-80	82-92	37.0-41.4	134-149				
14	81-89	93-103	41.5-46.1	150-166				
15	90-99	104-114	46.2-50.9	167-183				
16	100-108	115-125	51.0-56.0	184-201				
17	109-118	126-136	56.1-61.2	202-220	Hurricane	Hurricane	Air filled with foam; sea completely white with driving spray; visibility greatly reduced.	Very rarely experienced on land; usually accompanied by widespread damage.

To examine this question, a discussion of the logarithmic profile and its application to the marine boundary is required.

## The Viscous Sublayer

Flow over a smooth plate requires the velocity of the fluid to be zero at the surface of the plate. The change in average fluid velocity,  $\bar{u}(z)$ , with distance from the plate must be determined by the tangential shear stress. Newton's law of molecular viscosity states

$$\tau = \mu \, d\bar{u}(z)/dz = \rho \, \nu \, d\bar{u}(z)/dz. \quad (1)$$

At the interface this stress is referred to as the wall shear stress,  $\tau_w$ , and one can readily see by use of a Taylor series since  $\bar{u}(0) = 0$  that

$$\bar{u}(z) = \bar{u}(0) + (\partial\bar{u}/\partial z)_0 z + \dots \approx (\partial\bar{u}/\partial z)_0 z = (\tau_w/\rho)(z/\nu) = u_*^2 \delta_\nu. \quad (2)$$

In this expression  $u_*$  is the friction velocity at the surface and  $\delta_\nu$  is the thickness of the viscous sublayer. The relative importance of this viscous sublayer to the marine boundary layer can be determined by use of the Reynolds number ( $Re$ ), the ratio of the inertial forces (mechanical turbulence in the layer) to the viscous forces. This number can be expressed as  $Re = L_c \bar{u}/\nu$ , where  $L_c$  is the height of the marine layer (about 10–50 m),  $\bar{u}$  is the mean velocity of the air at a distance of (10 m) from the air–sea interface, and  $\nu$  is the fluid viscosity (about 0.002 m<sup>2</sup>/s); the resulting Reynolds number is  $5 \times 10^4$ , indicating turbulent flow. Since the corresponding viscous boundary layer thickness is (10<sup>−3</sup> m) much less than  $L_c$ , simple flat plate theory will by itself not be useful in describing the marine layer. However, the presence of mechanical, buoyancy, heat transport and mass transport, and sea surface motion effects can alter the near-surface profile.

## Mechanical Turbulence

One may account for the mechanical turbulence by using a coefficient of eddy viscosity,  $K_m$ , and treating the region between a reference distance near the interface,  $z_0$ , and the observed height of the turbulent layer.

$$\tau = \rho (\nu + K_m) d\bar{u}(z)/dz \cong \rho K_m d\bar{u}(z)/dz \quad z_0 < z < L_c \quad (3)$$

The resulting shear stress at the  $z_0$  reference condition becomes  $\tau_0 = \rho K_m (\partial\bar{u}/\partial z)_{z_0}$ .

The coefficient of eddy viscosity is known as the “austausch” or exchange coefficient,  $A = \rho K_m$ . Since the goal is to find the velocity profile, observe that  $d\bar{u}/dz$  depends on the parameters  $\nu$ ,  $z$ ,  $\rho$ , and  $\tau_0$ . The  $\pi$  theorem states that with these five

dimensional parameters and three fundamental dimensions, two nondimensional ratios can be derived as follows:

$$\begin{aligned}
 u_* &= \sqrt{(\tau_o/\rho)}, \text{ the friction velocity and the nondimensional ratios} \\
 &\quad (d\bar{u}/dz)(z/u_*) \text{ and } zu_*/\nu. \\
 \text{Dimensionless analysis yields } f_o((d\bar{u}/dz)(z/u_*), zu_*/\nu) &= 0 \\
 \text{or } d\bar{u}/dz &= (u_*/z)f_1(zu_*/\nu).
 \end{aligned} \tag{4}$$

The friction velocity,  $u_*$ , is necessary to determine the velocity profile. When the distance to the interface is small, such that all roughness elements are less than the reference distance  $z_{ov}$ , (see Fig. 2.2), the viscous effects determine the profile, and  $Re$  is of order 100, then  $z_{ov}$  is of order 1 mm and can only represent a smooth surface or completely still water. When the surface roughness is much larger than  $z_{ov}$ ,  $z_o$  is chosen sufficiently large enough to contain the surface roughness, as shown in Fig. 2.2; the larger-scale mechanical eddies dominate and the quantity  $f_1$  needs to be determined. Recognizing the weak dependence of  $f_1$  on  $zu_*/\nu$  when the reference distance ( $z_o$ ) is larger than the roughness ( $h_s$ ) of the interface, one takes the  $f_1$  function to be a constant,  $1/\kappa$ , where  $\kappa$  is von Kármán's constant. It then follows that

$$\begin{aligned}
 d\bar{u}/dz &= (u_*/z)(1/\kappa) \\
 \rightarrow u(z) &\cong (u_*/\kappa)\ln(z/z_o); \quad \bar{u}(z_o) = 0 \quad h_s < z_o < z < L_c
 \end{aligned} \tag{5}$$

In Eq. (5), the no-slip condition has been applied at the reference distance,  $\bar{u}(z_o) = 0$ , with  $z_o > h_s$ , the roughness distance. With a slight modification of the logarithmic argument,  $((z-h_s)/h_s)$ , the no-slip condition can be applied at the actual interface, but the distance,  $z_o$ , is small compared with the height of the marine layer and this modification has no practical importance.

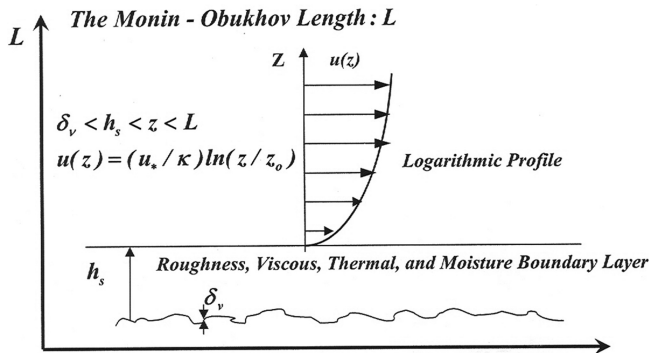


Fig. 2.2 The marine boundary layer for turbulent flow over a rough sea surface

## The Effect of Buoyancy

The viscous sublayer and the mechanical turbulence discussed thus far should be augmented by the incorporation of buoyancy effects. Mechanical turbulence is, by its nature, adiabatic, whereas buoyancy, by its nature, is diabatic and dependent on the vertical temperature variation, the lapse rate. When an air parcel is vertically displaced adiabatically, its volume will change in agreement with the ideal gas law, the adiabatic lapse rate. The buoyancy force for such a displacement is the difference between the parcel mass,  $M_p$ , and the displaced mass,  $M_a$ , times the gravitational acceleration ( $g$ ):

$$\begin{aligned} F_b &= g(M_a - M_p) = gV(\rho_a - \rho_p) = a_b M_p \\ \text{where } \rho_a, \rho_p &\text{ are the densities and } p/\rho = RT. \\ \rightarrow a_b &= g(\rho_a - \rho_p)/\rho_p = g(T_p - T_a)/T_a \end{aligned} \quad (6)$$

The buoyancy force yields buoyancy acceleration,  $a_b$ , the sign of which determines whether the force is positive, that is, upward, or negative, that is, downward. The adiabatic lapse rate,  $\Gamma$ , is thus the temperature change required by the decrease in pressure to maintain neutral buoyancy. The diabatic lapse rate,  $\gamma$ , is determined by the change of temperature resulting from volume change and heat exchange with the surrounding air. Expanding the temperatures in the above expression in a Taylor series about an equilibrium condition gives

$$a_b = g(\partial T_p/\partial z - \partial T_a/\partial z)\Delta z/T_a = g(\gamma - \Gamma)\Delta z/T_a. \quad (7)$$

This equation shows the importance of the adiabatic lapse rate,  $\Gamma$ ; when one has an adiabatic condition  $\gamma = \Gamma$ , a characteristic of the temperature stratification. When a diabatic lapse rate,  $\gamma$ , exists and normally it does, the buoyancy force can strongly affect the turbulence that occurs in the atmosphere when the production of turbulent energy by the wind stress is just large enough to counter the consumption by the buoyancy force.

This ratio of the consumption of turbulent energy by the buoyancy force to the production of turbulent energy by the wind stress is the Richardson number,  $R_i$ . If  $\Delta z=1$ , then

$$a_{bd} = g(\gamma - \Gamma)/T_a = (g/T_a)d\Theta/dz \quad (8)$$

and one has four fundamental quantities –  $d\bar{u}/dz$ ,  $d\Theta/dz$ ,  $g$ , and  $T_a$  – with three fundamental dimensions, so one nondimensional variable can be formed:

$$R_i = (g/T_a) \cdot \frac{d\Theta/dz}{(d\bar{u}/dz)^2} = (g/T_a) \cdot \frac{(\gamma - \Gamma)}{(d\bar{u}/dz)^2} \quad (9)$$

The importance of the adiabatic lapse rate and the relative importance of the diabatic lapse rate are observed. The quantitative values of the lapse rates are not as important

**Table 2.2** Thermal stability

1	$\gamma = -dTdz = \Gamma$	$T_p = T_a$	Neutral	The displaced air parcel neither rises nor falls
2	$\gamma > \Gamma$	$T_p > T_a$	Unstable	Vertical displacement is amplified by buoyancy
3	$\gamma < \Gamma$	$T_p < T_a$	Stable	Vertical displacement is dampened

as the relative differences. (The dry adiabatic lapse rate in the atmosphere is of order  $1^\circ\text{C}/100\text{ m.}$ ). Three cases of stability can be determined as neutral, unstable, and stable as shown in Table 2.2.

## The Influence of Heat Transport

The significant factor for heat transport is the departure of the eddy temperature from the temperature of the surrounding air. Because of this temperature difference, heat transfer can occur and thus eddies can transport heat across the flow. Just as the mechanical turbulence was described by a coefficient of eddy viscosity,  $K_m$ , one may also describe the heat transport,  $q$ , or flux by a coefficient of eddy heat conduction,  $K_q$ , with  $q = \rho K_q C_p (\gamma - \Gamma)$ , where  $C_p$  is the specific heat. The result is a modification of the Richardson number to a flux form:

$$R_f = R_i(K_q/K_m). \quad (10)$$

The number of fundamental quantities above has increased from four ( $z$ ,  $z_o$ ,  $u_*$ , and  $\kappa$ ) with the addition of  $g$ ,  $C_p$ ,  $\rho$ ,  $q$ , and  $T$  to nine. Dimensionless analysis will produce multiple nondimensional numbers and would be unnecessarily complex for the purpose of this treatment. A further simplification is thus required, such as that proposed by Lettau (1949) and latter by Monin and Obukhov (1953) [references from Slade (1968), Kitaigorodskii (1972), and Plate (1971)].

## The Monin–Obukhov Length

As shown in Fig. 2.2, the region of interest to our problem is that between some unspecified distance that encompasses the roughness of the surface,  $z_o \geq h_s$ , and heights specified by some empirical but characteristic length,  $L_c$ . In this region the flow can be considered stratified-parallel-turbulent flow from near the roughness distance to the specified characteristic height with constant stress and heat flux or a region with constant momentum and heat flow. With this assumption, the quantities of interest are  $g/T_a$ ,  $u_*$ , and  $K_q/C_p \rho$  and the Monin–Obukhov-derived unique length scale is

$$L = [u_*^3/\kappa(g/T_a)][-q_\Theta/C_p\rho]^{-1} = -u_*^3 C_p \rho T_a / \kappa g q_\Theta. \quad (11)$$

The Monin–Obukhov length,  $L$ , can be negative for unstable conditions, positive for stable conditions, and become infinite as  $\gamma \rightarrow \Gamma$ . The near-wall region can first be governed by viscous properties and then by additional turbulence by the interaction of the flow and the rough boundary. However, the dynamic layer between this roughness parameter and the characteristic length  $L_c = |L|$  because of the constant momentum, heat, and mass flux is a self-similar region with logarithmic profiles. The Richardson number now can be written as

$$\begin{aligned} R_{if} &= R_i K_q / K_m = (u_* Ta / \kappa g) (1 / L_c (d\bar{u}/dz)) \\ \text{and} \\ R_i &= [(g/\Theta) d\Theta/dz] / [d\bar{u}/dz]^2 = z/L_c \end{aligned} \quad (12)$$

where  $R_i = z/L_c$  is the local Richardson number. Thus, this complex problem (Fig. 2.2) of the marine boundary layer over a rough surface has been treated with a viscous sublayer,  $\delta_v$ , less than a roughness layer that contains the influence of viscous, thermal, and moisture sublayers,  $h_s$ , and a dynamic layer between this roughness layer and the Monin–Obukhov height. The velocity profile in this dynamic region with constant heat and momentum fluxes was shown to be

$$\begin{aligned} d\bar{u}(z)/dz &= u_*/\kappa z \\ \text{and} \\ \bar{u}(z) &= (u_*/\kappa) \ln(z/z_o) \quad \text{with} \quad \delta_v < h_s \leq z_o \leq z \leq L_c. \end{aligned} \quad (13)$$

This development, although not particularly quantitative, should provide a qualitative understanding of effect of the complex interaction of roughness, momentum, and heat transport on the development of the logarithmic profile.

## The Combined Influence of Mass, Momentum, and Heat Transport

Although the mass transfer due to moisture has not been included, it is sufficient to state that the laws of viscosity, heat conduction, and diffusion are all similar and for each phenomenon an eddy coefficient can be approximated and treated as has been done thus far. When all three effects, momentum, heat, and mass transfers, are considered, it is convenient to use relative quantities with the change in velocity between a reference height and the roughness height,  $\delta\bar{u} = \bar{u}(z_r) - \bar{u}(z_o)$ , the relative temperature difference,  $\delta\bar{\Theta} = \bar{\Theta}(z_o) - \bar{\Theta}(z_r)$ , and the specific moisture difference,  $\delta\bar{m}_e = \bar{m}_e(z_o) - \bar{m}_e(z_r)$ . The distance  $z_r$  is a reference distance and is usually taken to be a height of 10 m from the sea surface. The quantities of interest at this reference height are the momentum flux,  $\rho\bar{u}_r^2$ , the heat flux,  $\rho C_p \delta\bar{\Theta}\bar{u}_r$ , and the moisture-humidity flux,  $\rho\delta\bar{m}_e\bar{u}_r$ . Their description is based on the coefficients of drag,  $C_u$ , heat exchange,  $C_\Theta$ , and moisture exchange,  $C_{me}$ :



$$\begin{aligned}
C_u(z_r/h_s, z_r/L, h_s/\delta_v) &= \tau/\rho\bar{u}_r^2 \\
C_\Theta(z_r/h_s, z_r/L, h_s/\delta_\Theta, P_{R\Theta}) &= q_\Theta/\rho C_p \delta \bar{\Theta} \bar{u}_r \\
C_{me}(z_r/h_s, z_r/L, h_s/\delta_{me}, P_{Rme}) &= w_{me}/\rho \delta \bar{m}_e \bar{u}_r
\end{aligned} \tag{14}$$

The three sublayers for the conditions found near the sea surface result in Prandtl numbers ( $P_{R\Theta}$  and  $P_{Rme}$ ) of unity, and consequently

$$P_{R\Theta} = \delta_v/\delta_\Theta = \nu/\nu_\Theta = 1, \quad P_{Rme} = \delta_v/\delta_{me} = \nu/\nu_{me} = 1. \tag{15}$$

The result is the viscous, thermal, and moisture sublayers are approximately of equal thickness. These layers and the resulting roughness layer characterize the near-surface vertical transfer of momentum, heat, and moisture. Consequently, the coefficients only depend on three nondimensional ratios of  $z/h_s$ ,  $R_i$ , and  $R_e$ . The key result of this analysis can be summarized by use of nondimensionalized velocity, temperature, and moisture:

$$\tilde{u} = \bar{u}(z)/u_*; \quad \tilde{\Theta} = \bar{\Theta}(z)u_*/(-q_\Theta/\rho C_p), \quad \tilde{m}_e = \bar{m}_e \rho u_*/(-w_{me}). \tag{16}$$

The governing equation is

$$d\tilde{u}/dz = d\tilde{\Theta}/dz = d\tilde{m}_e/dz = 1/\kappa z; \quad \delta_v < h_s \cong z_o \leq z \leq L_c. \tag{17}$$

The coefficients are

$$\begin{aligned}
C_u(z/h_s, R_i, R_{es}) &= (\ln(z/z_o)/\kappa)^{-2} \\
C_\Theta &= C_u(z/h_s, R_i, R_{es})/(1 + C_u^{1/2} \delta \tilde{\Theta}) \\
C_{me} &= C_u(z/h_s, R_i, R_{es})/(1 + C_u^{1/2} \delta \tilde{m}_e) \\
C_u &\cong C_\Theta \cong C_{me} \quad z_o \leq z \leq L_c.
\end{aligned} \tag{18}$$

The final result is that in the dynamic marine layer these coefficients are approximately equal and are usually referenced to a height of 10 m.

The single factor of importance in the coefficients above besides the friction velocity is the roughness parameter,  $h_s$ . When the Reynolds number,  $R_e = h_s u_*/\nu = h_s/\delta_v$ , is large, the roughness parameter,  $z_o$ , is proportional to  $h_s$ , and the near-wall condition is roughness-controlled. When the Reynolds number is small, then the parameter  $z_o$  is comparable to  $\delta_v$  and the sea surface is calm and viscous forces dominate. Thus, the sea surface can be described as smooth, incompletely rough, and completely rough. In the completely rough case  $z_o = A_s h_s$ , where  $A_s$  is a constant factor depending on the steepness of the roughness.

## The Roughness Scale and Motion of the Surface

This treatment of the marine boundary layer has assumed that the surface is immobile and rigid. The rigid boundary condition may well be justified in light of the large density difference between air and water; however, the sea surface is definitely in motion. The supposition is that a quantitative treatment of the boundary layer is beyond the scope of this monograph, whereas a qualitative description that is useful in the characterization of oceanic ambient noise would be valuable. In this regard two factors are still to be discussed, the roughness and sea surface motion. Here the argument of Kitaigorodskii (1972) is useful. Although his treatment may not lend itself to a quantitative description of the boundary layer, the motion of the sea surface, and its roughness, it provides insight as to the role these various factors have in describing the characteristics of oceanic ambient noise.

The surface can be considered a rough surface with the roughness contained in a layer, the  $z_o$  roughness parameter, which is greater than the effective roughness and the viscous boundary layer as shown in Fig. 2.2. If a self-similar turbulence region is maintained up to this distance, the logarithmic velocity profile applies:

$$\bar{u}(z) = (u_*/\kappa) \ln(z/z_o) \quad \text{with} \quad \delta_v < h_s \leq z_o \leq z \leq L_c. \quad (19)$$

If the roughness of the surface waves moves downstream with a phase velocity of  $u_{wc}$  with an amplitude comparable to  $h_s$ , then in a Cartesian coordinate frame moving with the waves at velocity  $u_{wc}$ , the turbulent flow will be proportional to the relative motion:

$$\begin{aligned} \bar{u}(z) - u_{cw} &= (u_*/\kappa) \ln(z/z_o), \quad \delta_v < h_s \leq z_o \leq z \leq L_c \\ &\rightarrow u(z)/u_* = (1/\kappa) \ln(z/z_o) + u_{cw}/u_* \\ &= (1/\kappa) \ln(z/h_s \exp(-\kappa u_{cw}/u_*)). \end{aligned} \quad (20)$$

Thus, the motion of the boundary in this simple example can be incorporated in the logarithmic velocity profile by the inclusion of a factor  $h_s \cdot \exp(-\kappa u_{cw}/u_*) > \delta_v$ , a modification to the roughness parameter, an effective roughness parameter. This is not an exact solution to the boundary layer of a moving boundary, but states that the moving boundary presents a different near-surface condition because of its motion. If the amplitude  $h_s$  is the amplitude of the portion of the sea state spectrum  $S(\omega)$  in some interval  $d\omega$ , then the mean square roughness is

$$\begin{aligned} h_s^2(k) \cdot \exp(-2\kappa u_{cw}/u_*)/2 &= S(k)dk, \quad u_{cw} = g/\omega \\ \rightarrow \langle h_s^2 \rangle &= 2 \int_0^\infty S(k) \exp(-2\kappa u_{cw}(k)/u_*) dk \cong \langle z_o^2 \rangle \end{aligned} \quad (21)$$

The result is the simplest form of marine boundary layer including a rough moving surface. Undoubtedly, this equation may not, in general, describe the complicated near-surface condition, but it highlights the parameters that need be considered, such as the sea surface spectrum.

In summary, the logarithmic velocity profile has been applied to this marine layer problem following the approach of Kitaigorodskii (1972) that shows the wind stress coefficient is fundamentally dependent on three quantities:

$$C(z, u) = C(z/h_s, R_i, R_{es}), \quad (22)$$

where  $z$  is the observation point,  $h_s$  is the characteristic scale of the roughness,  $R_i$  is the Richardson number, and  $R_{es}$  is the Reynolds number for roughness. Kitaigorodskii also showed, for a moving boundary under neutral stability conditions, that

$$u(z)/u_* \simeq 1/\kappa \ln(z/h_s) = C(z, u(z))^{-1/2}, \quad (23)$$

where  $u_* = \sqrt{(\tau/\rho)}$  is the friction velocity,  $\kappa$  is von Kármán's universal constant, and  $h_s$  is given by

$$h_s \simeq [2 \int_0^\infty S(k) \exp(-2\kappa u_{cw}(k)/u_*) d\omega]^{1/2} \quad (24)$$

with  $S(\omega)$  being the frequency spectrum of the wave field.

In general, the wind stress coefficient is dependent on the stability of the boundary layer (mechanical turbulence, heat and mass transport) as well as the roughness scale modified by the motion. This roughness scale depends on the sea state spectrum, which in turn is a function of time, the wind at a given speed, and the fetch. These fundamental considerations clearly indicate that wind speed alone may not simply be the best indicator of the state of the sea. As will be observed in later sections, satellite and large-scale meteorological observations can be used to correctly parameterize the state of the sea.

## A Summary of the Wind Stress Coefficient and Critical Friction Velocity

Boundary layer investigations employ a standard measurement height of 10 m. The wind stress coefficient at this reference point is  $C_{10}(U_{10})$  and is related to  $u_*$  with use of the previously discussed logarithmic velocity profile. The variables such as wind speed,  $U_{10}$ , and Richardson number are also referenced to this height. Amorcho and DeVries (1980) examined many boundary measurements by plotting  $C_{10}$  and  $u_*$  versus  $U_{10}$  for a wide range of wind speed conditions. The results are shown in Fig. 2.3. In general, they found three distinct wind speed regions. The first region is found prior to the onset of wave breaking with  $C_{10}$  constant. The second region, labeled as a transition region, is for wind speeds between 7 and 20 m/s. In this region, both  $u_*$  and  $C_{10}$  have nonlinear dependencies on wind speed. Finally, for wind speeds greater than 20 m/s, there is a saturation region with  $C_{10}$  becoming relatively constant.

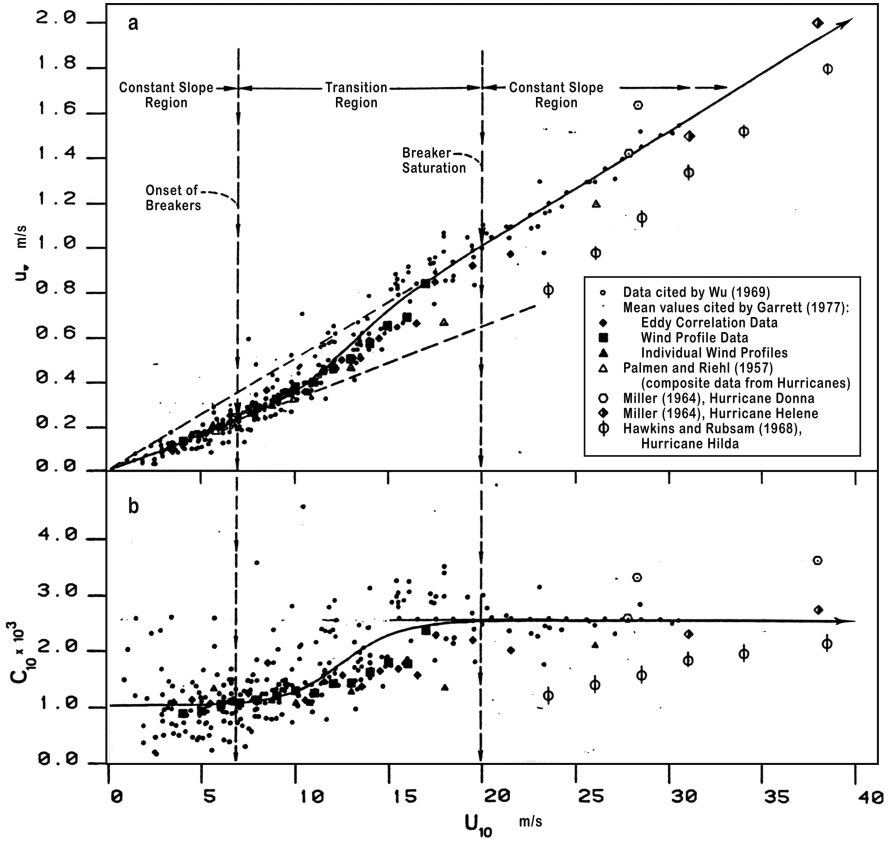


**Fig. 2.3** Estimates of the friction velocity and wind stress coefficient from measurements over water surfaces

## Friction Velocity and Breaking Waves

An important feature of this summary is the importance of wave breaking. Kerman states that this wave breaking occurs when the kinetic energy of an eddy near the surface,  $\rho l_e^3 u_*^2$ , can overcome the surface tension of the water,  $l_e^2 T_{sur}$ . If the limiting acceleration for convective overturning of the crest is taken as  $l \approx u_*^2/g$ , then a critical friction velocity  $u_{c*}^4 = 4 g T_{sur}/\rho$  can be defined such that when the friction velocity exceeds this value waves begin to break. This expression for the critical friction velocity is also the minimum phase velocity of the gravity–capillary waves. The relationships discussed thus far are qualitative and need not be quantitative for the description of environmental measurements necessary for oceanic ambient noise studies. However, it should be clear at this point that wind speed alone will not suffice. To stress the importance of this wave-breaking phenomenon, Fig. 2.4 shows a breaking wave observed by Su (1984).

Brackish water measurements, such as the experiments by Su (1984) with three-dimensional waves (Fig. 2.4), show a typical sequence of events: from the initial wave breaking; to the formulation of a columnar bubble plume; to a more diffuse cloud swept by the subsurface orbital motion; and finally to dispersion of near-surface bubbly features. Although freshwater experiments may be useful in visualizing the sequence, the bubbly mixture in these types of experiments appears to be composed of larger bubbles, faster rise times, and consequently different acoustic characteristics. The difference in the bubble sizes and rise times also may result in different sound production mechanisms.

Thorpe (1982, 1983, 1986) and his colleagues performed a series of experiments with upward-looking sonar in lakes and in the deep ocean. He observed that bubble clouds were convected to meter depths by wave-breaking turbulence and vorticity with subsequent ordered patterns consistent with Langmuir circulation. Thorpe's results showed an exponential decrease in volume scatter strength with depth, a mean depth of penetration that was proportional to  $U_{10}$  and the air-water temperature difference ( $\Delta\theta_{AW}$ ). Different cloud characteristics for stable ( $\Delta\theta_{AW} > 0$ ) and unstable ( $\Delta\theta_{AW} < 0$ ) conditions were also observed. For example, the stable condition was found to result in a "billowy" cloud structure, whereas the unstable condition resulted in a columnar characteristic. This observation is reinforced by the parametric dependence of the logarithmic profile on  $R_i$  previously discussed. Observations by Crawford and Farmer (1987) confirmed these breaking-wave effects: the exponential distribution of bubble density with an "e folding" depth between 0.7 and 1.5 m, a bubble density variation with  $u_{10}^{3 \pm 0.3}$ , a weak dependence on the Langmuir circulation, and "v"-shaped columnar clouds for ( $\Delta\theta_{AW} < 0$ ).

Thorpe also observed pronounced differences in clouds produced by wave breaking in freshwater and salt water. He attributed these differences to chemical effects discussed by Scott (1975) to explain Monahan's (1971) observation concerning freshwater whitecaps. That is, under nearly identical physical conditions, bubble distributions produced in salt water have a smaller mean radius and a larger number of bubbles. According to Scott (1986), surface chemical effects can be an important factor preventing coalescence, and "significant differences observed in the duration of freshwater and salt water whitecaps may be ascribed to these effects." Bubbles in salt water were greater in number, smaller, more densely packed, carried deeper, and slower to rise to the surface than those formed in freshwater by a similar wave-breaking event.

Pounder (1986) showed a distinct temperature-dependent difference between distilled water (coalescence occurs) and salt water (coalescence does not occur). He attributed this difference to an ionic effect. Pounder's laboratory observations support the conclusion drawn by Scott and Thorpe that microbubble distributions result from salt water wave breaking.

Bubble size measurements [made by Medwin (1977), Kolovayev (1976), Johnson and Cooke (1979), Bouguel (1985), and Crawford and Farmer (1987) and then reviewed by McDaniel (1987) and Carey and Fitzgerald (1990)] had bubble radius distributions between 50 and 70  $\mu\text{m}$  and an exponential numerical decrease

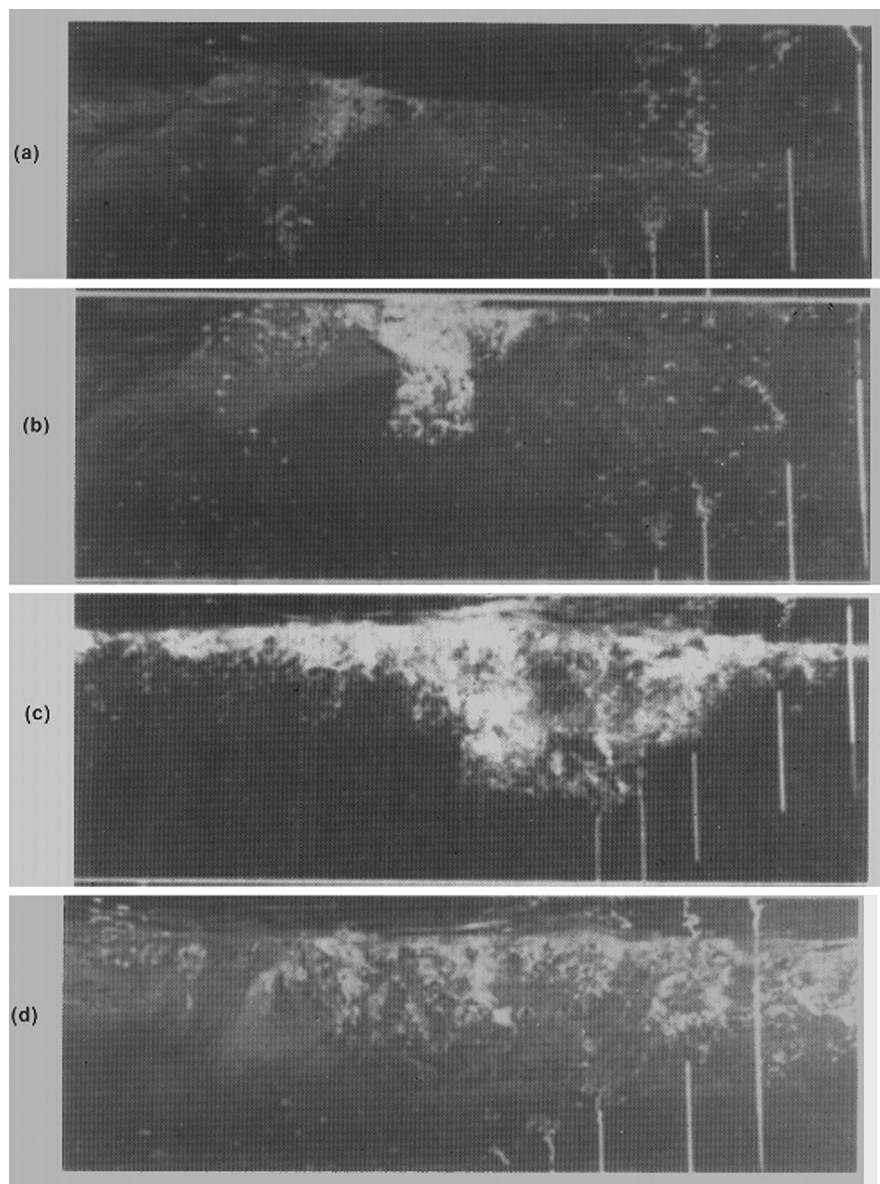


**Fig. 2.4** Three-dimensional crescent-shaped breakers that resemble deepwater oceanic breakers are viewed in 2-s intervals from under the breaking wave. The vertical strings are spaced at 30.5-cm intervals and have 15.3 white and black sections. The wave steepness, the initial amplitude  $a_0$  times the initial wavenumber  $k_0$ , is 0.33. Su (1984)

with an increase in radius. Kolovayev observed that at wind speeds of 13 m/s, all bubbles were less than 350  $\mu\text{m}$ . The distribution maximum was found to shift to larger radii with increasing wind speed and depth.

Monahan (1990) developed a description of the evolution of a bubble plume and cloud from a breaking wave consistent with these results. Shown in Fig. 2.5 are the results of his analysis for a wind speed of 13 m/s. The  $\alpha$  plume, first panel, occurs within 1–2 s of the breaking event and its characteristic depth is 0.5 m with a volume fraction of  $4 \times 10^{-2} - 8 \times 10^{-2}$  on the basis of the extrapolated bubble size distribution for the  $\beta$  plume. The second panel shows his “ $\beta$ ” plume, a bubble size distribution derived from his aerosol generation model, and a bubble size distribution based on the measurements of Johnson and Cooke (1979). The  $\beta$  plume is estimated to have duration between 1 and 10 s and a volume fraction based on an integrated size distribution of  $1 \times 10^{-4} - 2 \times 10^{-4}$ . In the third panel, the characteristic of the cloud has a bubble size distribution consistent with the measurements of Johnson and Cooke and a scaling based on cloud sea surface ocean to whitecap area of 25:1. The duration of this feature is estimated to be on the order of 100 s and the average volume fraction is between  $10^{-6}$  and  $10^{-7}$ .

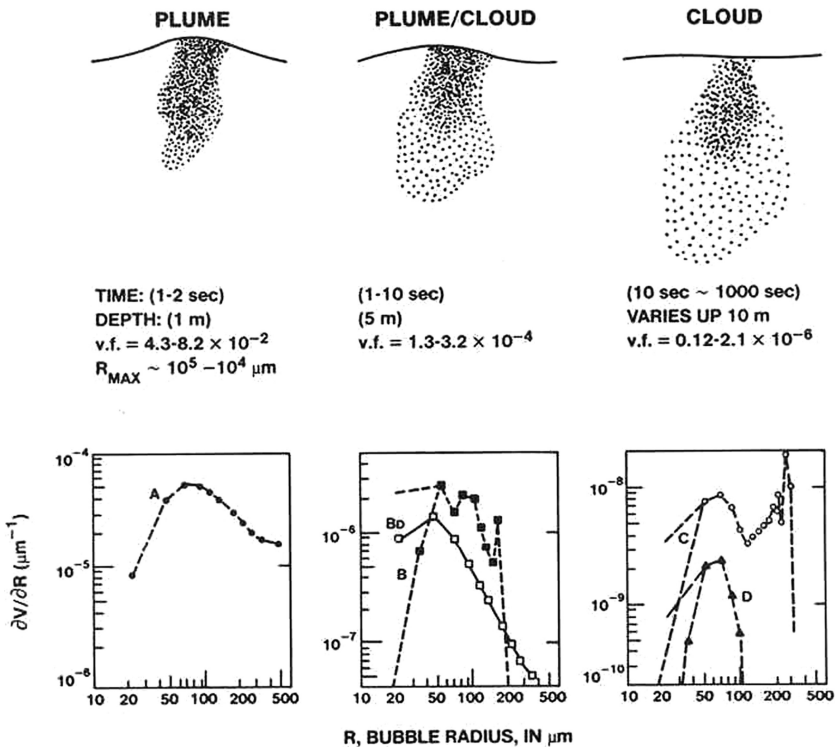


**Fig. 2.5** Evolutionary model of a wave-breaking bubble plume and cloud as a sequence of temporal samples covering time periods of 1, 10, and 100 s Monahan (1989)



The measurement of the bubble size distribution, void fraction, and spatial characteristics of bubble clouds and plumes has been shown to be difficult. Nevertheless, general characteristics have emerged concerning breaking waves, the determination of the subsurface characteristics, and the temporal evolution of these features.

Monahan used exponential variation in depth, cross-sectional area, and time with measured “e folding” characteristics to scale the results for the  $\alpha$ ,  $\beta$ , and  $\gamma$  plumes. These features are shown schematically in Fig. 2.6 as a qualitative picture of the near-surface boundary condition to guide sound scattering and noise measurements.

The surface manifestation of the active-stage class A whitecap (Fig. 2.6) lends itself to observation by shipboard and airborne observation as well as satellite measurement. This whitecap appearance was the basis for the previously discussed

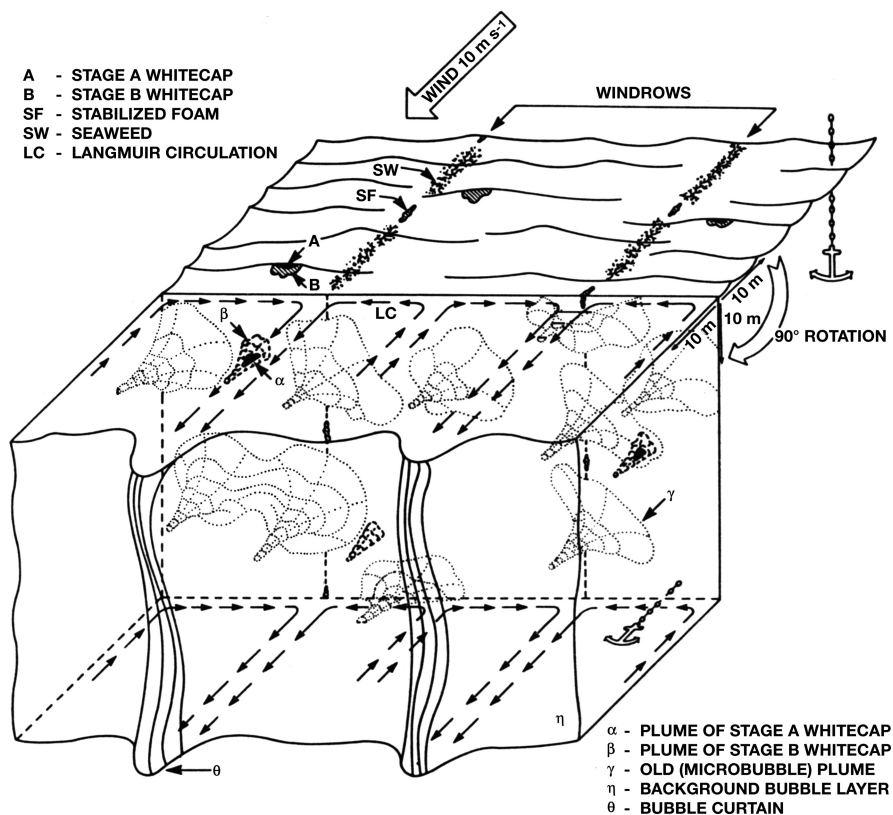


**Fig. 2.6** Surface view and a subsurface view, rotated by  $90^\circ$ . The anchor-cum-plumb bobs are included to show the vertical direction on both cuts. The visual manifestation on the sea surface is the whitecap produced by the spilling breakers, nominally a wind speed greater than 4 m/s. Also shown are the scale depths of the subsurface characteristics organized by the Langmuir circulation



Beaufort scale used by Wenz. Satellite-sensed microwave backscatter may well be a viable means of automatically sensing the sea state by the scattering from the active whitecaps and has been proposed by both Monahan and Kerman. The class A active whitecaps and concentrated  $\alpha$  bubble plumes are of short duration and acoustically significant. The second feature shown in this figure is the older class B whitecap, the hazy foam patch that remains after the wave has passed. These features cover a wider area and have a microwave emissivity that can be observed with multichannel microwave radiometers. Monahan (1990) discussed the characteristics in detail. The whitecap coverage and Beaufort scale are related, and combine the heat mass and transport effects into an observable parameter.

## The Whitecap Index

Wilson (1983) found that ambient noise levels varied in proportion to the “whitecap” index,  $W(u)$ , of Ross and Cardone (1974) and proposed three regions of wind speed dependency as shown in Table 2.3.

**Table 2.3** The Whitecap index

I	$W(u) = 0$	$u < 4.5 \text{ m/s}$
II	$W(u) = (4.6 \times 10^{-3})U^3 - (4.9 \times 10^{-2})U^2 + (4.63 \times 10^{-1})U - 1.5$	$4.5 < U < 15 \text{ m/s}$
III	$W(u) = (20.97)(U/15)1.5$	$15 \text{ m/s} < U$

Wu (1980) stated that the whitecap index  $W(u)$  should be related to the energy flux of the wind under equilibrium conditions. The energy flux ( $\dot{E}$ ), or the rate of doing work, is related to the wind stress ( $\tau$ ) and a surface drift current ( $V$ ):

$$W(U_{10}) \propto \dot{E} = \tau V \propto \tau U_* \propto C_{10}^{3/2} U_{10}^3, \quad (25)$$

where  $W(U_{10})$  is the percentage of the sea surface covered by whitecaps,  $\tau$  is the shear stress at the surface,  $U_*$  is the friction velocity, and  $U_{10}$  is the 10-m-elevation wind speed. This relationship between the whitecap index and the wind stress coefficient  $C_{10}$  ties the whitecap index to fundamental parameters governing the exchange of momentum, mass, and energy in the sea surface interaction zone.

The whitecap index can be obtained either by measuring the index directly or by estimating the wind stress coefficient from boundary layer measurements. Monahan (1990) [see also O’Murchartaigh and Monahan (1986), Monahan and O’Murchartaigh (1981)] determined the wind speed variation of the whitecap index by fitting

$$W(U_{10}) = \alpha U_{10}^\lambda \quad (26)$$

to measured fractional whitecap coverage. Monahan found that  $\lambda = 3.41$  provided the best fit to all data, with individual sets of data yielding values of  $\lambda$  between 2.55

and 3.75. Monahan also proposed classifying whitecaps as class A, young, and class B, old.

Wu (1981, 1986) contended that  $C_{10}(U_{10}) \propto U_{10}^{1/2}$ , and consequently a variation of  $W$  with  $U^{3.75}$ . However, Wu (1980) earlier recommended a linear dependence of  $C_{10}(U_{10})$  on wind speed. His review of measured wind stress coefficients as a function of  $U_{10}^{3m}$  showed most values of  $m$  between 1 and 1.3 [also, see Large (1981), Donelan (1982), and Smith (1980)]. The reader is cautioned concerning the use of relationships between the whitecap index and the wind stress coefficient  $C_{10}(U_{10})$  such as the qualitative relationships shown in Fig. 2.7 as investigations are continuing and a quantitative relationship has not been developed.

The results shown in Fig. 2.7 are remarkably similar to the acoustic noise level characteristics. Most observations of noise are in the 7–20-m/s wind range, thus a wind speed dependency similar to the variation in wind stress coefficient can be expected. Since the wind stress coefficient depends on the logarithmic profile and, in turn, on the Reynolds and Richardson numbers, the sea state spectrum, and the friction velocity, ambient noise levels may also have these characteristics. Thus,

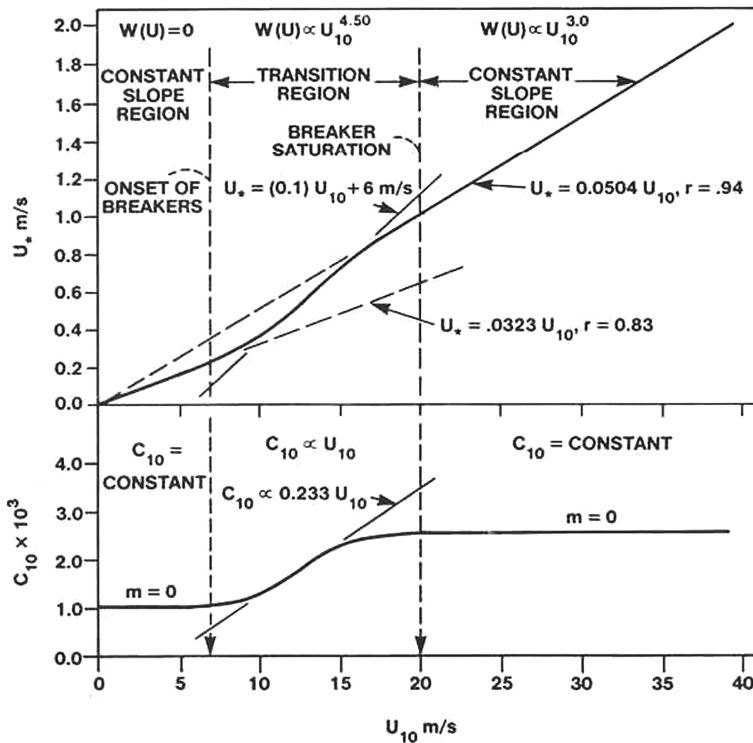


**Fig. 2.7** Summary of the relationships for the wind stress coefficient at 10 m,  $C_{10}$ , and the estimated friction velocity,  $u_*$ , versus the 10-m wind speed,  $u_{10}$ , with whitecap indexes,  $W(u_{10}^m)$ , delineated

one may conclude that ambient noise measurements should be performed that concurrently measure the wind speed ( $U_{10}$ ), the air–water temperature difference as a simplified  $R_i$  measure, the sea state spectrum as an indicator of roughness, and the moisture content necessary for correct estimation of  $R_e$ . The measurement of whitecaps by the use of satellite observations, satellite estimates of the 10-m wind speed and large-scale meteorological computational tools may be useful in the calculation of wind-induced ambient noise.

## References and Suggested Readings

- Amorocho, J. and J. J. DeVries (1980). “A new evaluation of the wind stress over water surfaces” J. Geophys. Res. 85(C1): 433–442.
- Bouguel, M. and S. Baldy (1985). “Measurement of bubbles in a stationary field of breaking waves by a laser-based single-particle scattering technique.” J. Geophys. Res. 90(C1): 1037–1047.
- Bowditch, N. (1966). *American Practical Navigator*. U.S. Navy Hydrographic Office, Government Printing Office (H.O. Pub. No. 9), Washington, DC.
- Carey, W. M. and J. W. Fitzgerald (1990). Low frequency noise from breaking waves. In *Natural Physical Sources of Underwater Sound*. Cambridge, UK. B. R. Kerman (Ed.), Kluwer Academic Publishers, Dordrecht (1993), pp. 277–304.
- Crawford, G. B. and D. M. Farmer (1987). “On the spatial distribution of ocean bubbles.” J. Geophys. Res. 92(8): 8231–8243.
- Donelan, M. A. (1982). The dependence of Aerodynamic Drag Coefficient on Wave Parameters. Proceedings of the 1st Conference of Meteorology and Air Sea Interaction of the Coastal Zone, American Meteorological Society, pp. 381–387.
- Hinze, J. O. (1959). *Turbulence*. McGraw-Hill Book Co., NY, pp. 13–25.
- Johnson, B. D. and R. C. Cooke (1979). “Bubble populations and spectra in coastal waters: A photographic approach” J. Geophys. Res. 84(C7): 1038–1042.
- Kerman, B. R. (1984). “Underwater sound generation from breaking waves.” J. Acoust. Soc. Am. 75(1): 149–164.
- Kitaigorodskii, S. A. (1972). *The Physics of Air-Sea Interaction*. U.S. Department of Commerce, NTIS, Springfield, VA.
- Kolovayev, P. D. (1976). “Investigation of the concentration and statistical size distribution of wind produced bubbles in the near surface ocean layer.” *Oceanology* 15: 659–661.
- Large, W. G. and S. Pond (1981). “Open ocean momentum flux measurement in moderate to strong winds.” J. Phys. Oceanogr. 11: 324–336.
- McDaniel, S. T. (1987). Subsurface Bubble Densities from Acoustic Backscatter Data, ARL/TM-87-57, Applied Research Lab, Pennsylvania State University, State College, PA.
- Medwin, H. (1977). “In situ acoustic measurements of microbubbles at sea.” J. Geophys. Res. 82(6): 971–976.
- Monahan, E. C. (1971). “Oceanic whitecaps.” J. Phys. Oceanogr. 1: 138–144.
- Monahan, E. C. (1988). Whitecap coverage as a remotely monitorable indication of the rate of bubble injection into the oceanic mixed layer. In *Sea Surface Sound*. B. R. Kerman (Ed.), Kluwer Academic Publishers, Boston, pp. 85–86.
- Monahan, E. C. and M. Lu (1990). “Acoustically relevant bubble assemblages and their dependence on meteorological parameters.” IEEE J. Ocean. Eng. 15(4): 340–349.
- Monahan, E. C. and I. O’Murchartaigh (1981). “Optimal power-law description of oceanic whitecap coverage dependence on wind speed.” J. Phys. Oceanogr. 10: 2094–2099.
- Monahan, E. C. and T. Torgersen (1991). The enhancement of air sea gas exchange by oceanic whitecapping. In *Air-Water Mass Transfer*. S. C. Wilhelms and J. S. Gulliver (Eds.), American Society of Civil Engineers, New York, NY, pp. 608–617.

- Monahan, E. C. and M. A. Van Patten (Eds.) (1989). *The Climate and Health Implications of Bubble-Mediated Sea-Air Exchange*. Connecticut Sea Grant College Program, University of Connecticut at Avery Point, Groton, CT.
- Monahan, E. C. and C. R. Zietlow (1969). "Laboratory comparisons of fresh-water and salt-water whitecaps." *J. Geophys. Res.* 74: 6961–6966.
- O'Murcheartaigh, I. G. and E. C. Monahan (Eds.) (1986). *Oceanic Whitecaps*. D. Reidel Publishing Co., Boston, MA.
- Plate, E. J. (1971). *Aerodynamic Characteristics of the Atmospheric Boundary Layers*. U.S. Atomic energy Commission, Available NTIS-TID-25465, National Technical Information Service, U.S. Dept. of Commerce, Springfield, VA.
- Pounder, C. (1986). Sodium chloride and water temperature effects on bubbles. In *Oceanic Whitecaps*. E. C. Monahan and G. MacNiocaill (Eds.), Reidel, Dordrecht, Holland, p. 278.
- Ross, D. B. and B. Cardone (1974). "Observations of oceanic whitecaps and their relation to remote measurements of surface wind speed." *J. Geophys. Res.* 79: 444–452.
- Scott, J. C. (1975). "The of salt in whitecap persistence." *Deep Sea Res. Oceanogr. Abstr.* 22(10): 653–654.
- Scott, J. C. (1986). The effects of organic films on water surface motions. In *Oceanic Whitecaps*. E. C. Monahan and G. MacNiocaill (Eds.), Reidel, Boston, pp. 159–165.
- Slade, D. H. (1968). *Meteorology and Atomic Energy*. U.S. Atomic energy Commission, Available NTIS-TID-24190, National Technical Information Service, U.S. Department of Commerce, Springfield, VA.
- Smith, S. D. (1980). "Wind stress and heat flux over the ocean in gale force winds." *J. Phys. Oceano.* 10: 709–726.
- Smith, S. D. (1981). "Comment on "A new evaluation of the wind stress coefficient over water surfaces"." *J. Geophys. Res.* 86(C5): 4307.
- Su, M. Y. (1984). Experimental studies of surface wave breaking and air entrainment. In *Gas Transference at Water Surfaces*. W. Brutsaert and G. Jirka (Eds.), Reidel Press, Dordrecht, pp. 211–219.
- Thorpe, S. A. (1982). "On the clouds of bubbles formed by breaking wind-waves in deep water, and their role in air-sea gas transfer." *Phil. Trans. Roy. Soc. Lond.* A304: 155–210.
- Thorpe, S. A. (1983). Bubble clouds: A review of their detection by sonar, of related models, and of how Kv may be determined. In *Oceanic Whitecaps and Their Role in Air-Sea Exchange Processes*. E. C. Monahan and G. MacNiocaill (Eds.), Reidel in association with Galway University Press, pp. 57–68, 1986.
- Thorpe, S. A. (1986). "Measurements with an automatically recording inverted echo sounder: Aries and bubble clouds." *J. Phys. Ocean.* 16: 1462–1478.
- Urlick, R. J. (1984). *Ambient Noise in the Sea*, Undersea Warfare Technology Office, NAVSEA, D.O.N., Washington, DC (Also available from Peninsula Publishing, Los Altos, CA, 1986.).
- Wenz, G. M. (1962). "Acoustic ambient noise in the ocean: Spectra and sources." *J. Acoust. Soc. Am.* 34: 1936–1956.
- Wilson, J. H. (1983). "Wind-generated noise modeling." *J. Acoust. Soc. Am.* 73(1): 211–216.
- Wu, J. (1980). "Wind-stress coefficient over sea surface near neutral conditions – a revisit." *J. Phys. Oceano.* 10: 727–740.
- Wu, J. (1981). "Bubble populations and spectra in the near-surface ocean: Summary and review of field measurements." *J. Geophys. Res.* 86(C1): 457–463.
- Wu, J. (1985). "Parameterization of wind-stress coefficients over water surfaces." *J. Geophys. Res.* 90(C5): 9069–9072.
- Wu, J. (1986). Whitecaps, bubbles, and spray. In *Oceanic Whitecaps*. E. C. Monahan and G. MacNiocaill (Eds.), D. Reidel Publishing Co., Boston, MA, pp. 113–123.



<http://www.springer.com/978-1-4419-7831-8>

Ocean Ambient Noise  
Measurement and Theory  
Carey, W.M.; Evans, R.B.  
2011, XIV, 266 p., Hardcover  
ISBN: 978-1-4419-7831-8